RESEARCH ARTICLE | DECEMBER 11 2023

Phase synchronization in a sparse network of randomly connected neurons under the effect of Poissonian spike inputs

Special Collection: Nonlinear dynamics, synchronization and networks: Dedicated to Jürgen Kurths' 70th birthday

Bruno R. R. Boaretto ; Paulo R. Protachevicz ; Matheus Hansen ; Jonas Oliveira ; Alexandre C. Andreani ; Elbert E. N. Macau

Chaos 33, 123115 (2023)
https://doi.org/10.1063/5.0179912

Phase synchronization in a sparse network of randomly connected neurons under the effect of Poissonian spike inputs

Cite as: Chaos 33, 123115 (2023); doi: 10.1063/5.0179912
Submitted: 5 October 2023 · Accepted: 13 November 2023 ·
Published Online: 11 December 2023

Bruno R. R. Boaretto,[1,a)] Paulo R. Protachevicz,[2,3] Matheus Hansen,[4] Jonas Oliveira,[5] Alexandre C. Andreani,[1,6] and Elbert E. N. Macau[1,b)]

AFFILIATIONS

[1]Institute of Science and Technology, Universidade Federal de São Paulo, 12247-014 São José dos Campos, São Paulo, Brazil
[2]Physics Institute, University of São Paulo, 05508-090 São Paulo, São Paulo, Brazil
[3]Institute for Complex Systems and Mathematical Biology, SUPA, University of Aberdeen, AB24 3UE Aberdeen, United Kingdom
[4]Center for Mathematics and Applications (NOVA Math), NOVA School of Science and Technology, Universidade NOVA de Lisboa, Quinta da Torre, 2829-516 Caparica, Portugal
[5]National Institute for Space Research, 12227-010 São José dos Campos, São Paulo, Brazil
[6]Federal Institute of São Paulo, 12322-030 Jacareí, São Paulo, Brazil

Note: This paper is part of the Focus Issue on Nonlinear dynamics, synchronization and networks: Dedicated to Juergen Kurths' 70th birthday.
[a)]**Author to whom correspondence should be addressed:** bruno.boaretto@unifesp.br
[b)]Co-senior author

ABSTRACT

This article investigates the emergence of phase synchronization in a network of randomly connected neurons by chemical synapses. The study uses the classic Hodgkin–Huxley model to simulate the neuronal dynamics under the action of a train of Poissonian spikes. In such a scenario, we observed the emergence of irregular spikes for a specific range of conductances and also that the phase synchronization of the neurons is reached when the external current is strong enough to induce spiking activity but without overcoming the coupling current. Conversely, if the external current assumes very high values, then an opposite effect is observed, i.e., the prevention of the network synchronization. We explain such behaviors considering different mechanisms involved in the system, such as incoherence, minimization of currents, and stochastic effects from the Poissonian spikes. Furthermore, we present some numerical simulations where the stimulation of only a fraction of neurons, for instance, can induce phase synchronization in the non-stimulated fraction of the network, besides cases in which for larger coupling values, it is possible to propagate the spiking activity in the network when considering stimulation over only one neuron.

The cooperative behavior of neurons and neuronal areas associated with synchronization proves to be a fundamental neural mechanism and is relevant to many cognitive processes. The brain operates in a dynamic environment with spontaneous activity, generating unpredictable action potentials in neurons. In this scenario, neurons are submitted to a wide diversity of inputs that are provided, for example, from ion channel flux to coupling interactions and external perturbations. Hence, the effect of stimulation and perturbation protocols on the spiking activity is a key topic of relevance to neuroscience being the focus of several works in the last few decades. This research article aims to investigate the emergence of phase synchronization in a network of randomly connected neurons under the effect of a train of Poissonian spikes. The appearance of phase synchronization is explained by analyzing the competition between internal and external currents in the network, as well as considering the Poisson inputs only in a fraction of the neuronal network. The results shed light on the emergence mechanism behind synchronous and asynchronous activities in neuronal networks under stochastic stimuli.

I. INTRODUCTION

The human brain is an intricate system composed of approximately 10^{11} neurons connected by 10^{15} synapses.[1] Understanding the relationship between the spatiotemporal activity patterns of neurons and brain functions is a primary objective of neuroscience. The complexity of the brain arises from the cooperative interaction among neurons in response to external stimuli, which leads to spontaneous activation patterns.[1]

In this work, we study the phase-synchronization features of a sparse network of randomly connected neurons under the effect of a train of Poissonian spikes. These types of spike inputs are thought to play an important role in generating the highly irregular spiking patterns observed in cortical neurons.[2,3] There are several lines of evidence that support the use of Poissonian spike inputs in cortical neurons.[2–6] One of the key pieces of evidence comes from studies of the statistics of natural stimuli, such as images or sounds.[7] These studies have shown that the statistical properties of natural stimuli are well-described by Poisson processes, suggesting that the brain may have evolved to process information in a way that is optimized for these statistics.[5,8,9]

To simulate the neuronal dynamics, we use the classic Hodgkin–Huxley model,[10] which mimics the action potential when the neuron is stimulated above a threshold.[11] The model exhibits Hopf bifurcations as the constant inputted current is varied,[11,12] in which for a range of currents, there is a stable limit cycle that gives rise to periodic spiking behavior.[13] We show that the behavior induced by Poissonian spikes consists of irregular spikes for a specific range of conductances. As the main result, we identified the appearance of high firing frequency and synchronization in the network considering different fractions of Poissonian perturbed neurons. Our findings highlight the influence of stochastic external stimuli (Poissonian) and internal neuronal interactions (coupling) on the brain's emergence of complex firing patterns.

The neuronal activity characterized by the action potential occurs due to a process of depolarization followed by repolarization when neurons are sufficiently stimulated.[11] When two or more neurons start their depolarization process together, the behavior can be attributed to the collective phenomenon that is associated with the more general framework of phase synchronization of oscillators.[14] All the behavioral disorders that characterize psychiatric illness (unhealthy neural behaviors) are disturbances in brain functioning,[1] and abnormal levels of synchronization have been related to unhealthy neural behaviors, such as epilepsy and Parkinson's disease.[1,15–17]

The main goal of this study is to investigate the emergence of phase synchronization in a network of randomly connected neurons under the influence of a train of Poissonian spikes. Our primary objective is to understand the mechanisms underlying synchronization and how they are affected by the balance between external currents and coupling interactions.

We also consider the impact of selective patterns of stimulation received by different brain areas, which reflect their specialized functions and unique connectivity profiles within the neural network.[1] By selectively stimulating subpopulations within the network, including the use of techniques, such as optogenetics,[18,19] we can gain insights into localized effects on synchronization and network-level properties.[20] This approach allows us to explore the functional roles, interactions, and contributions to network behavior, providing a comprehensive understanding of how different brain areas interact and synchronize within the neural network.

This paper is organized as follows: Sec. II presents the neuronal model and the equations that rule the external synaptic current, Sec. III presents the network setup and how the phase synchronization is evaluated, the results are depicted in Sec. IV, and Sec. V presents the discussion and our conclusions.

II. NEURONAL MODEL

To simulate the spiking neuronal dynamics, we consider the Hodgkin–Huxley (HH) model,[10] which was the first to describe mathematically a regenerative current that generates an action potential. The time evolution of the membrane potential of the neuron $V(t)$ measured in mV (millivolts) is related to the variations of two voltage-gated channels associated with the ion concentrations of potassium (K^+) and sodium (Na^+), as well as a leakage channel associated with the passive variations (non-gated channels).[13] The time evolution of the membrane potential of the neuron $V(t)$ is given by

$$C_M \frac{dV}{dt} = -g_K n^4 (V - E_K) - g_{Na} m^3 h (V - E_{Na}) - g_\ell (V - E_\ell) + I_{ext}(t), \tag{1}$$

$$\frac{dn}{dt} = \alpha_n (1 - n) - \beta_n n, \tag{2}$$

$$\frac{dm}{dt} = \alpha_m (1 - m) - \beta_m m, \tag{3}$$

$$\frac{dh}{dt} = \alpha_h (1 - h) - \beta_h h, \tag{4}$$

where C_M is the capacitance of the cell membrane and I_{ext} is the external current. The parameters g_K, g_{Na}, and g_ℓ are the maximum conductances, and E_K, E_{Na}, and E_ℓ are the reversal potential of each ionic current. The variables n and m are related to the activation of the potassium and sodium ionic currents, respectively, and h is the inactivation of the sodium current. α and β are functions dependent on $v = V/\text{mV}$ described as

$$\alpha_n = \frac{0.01(v + 55)}{(1 - \exp[-(v + 55)/10])}, \tag{5}$$

$$\alpha_m = \frac{0.1(v + 40)}{(1 - \exp[-(v + 40)/10])}, \tag{6}$$

$$\alpha_h = 0.07 \exp[-(v + 65)/20], \tag{7}$$

$$\beta_n = 0.125 \exp[-(v + 65)/80], \tag{8}$$

$$\beta_m = 4 \exp[-(v + 65)/18], \tag{9}$$

$$\beta_h = \frac{1}{(1 + \exp[-(v + 35)/10])}. \tag{10}$$

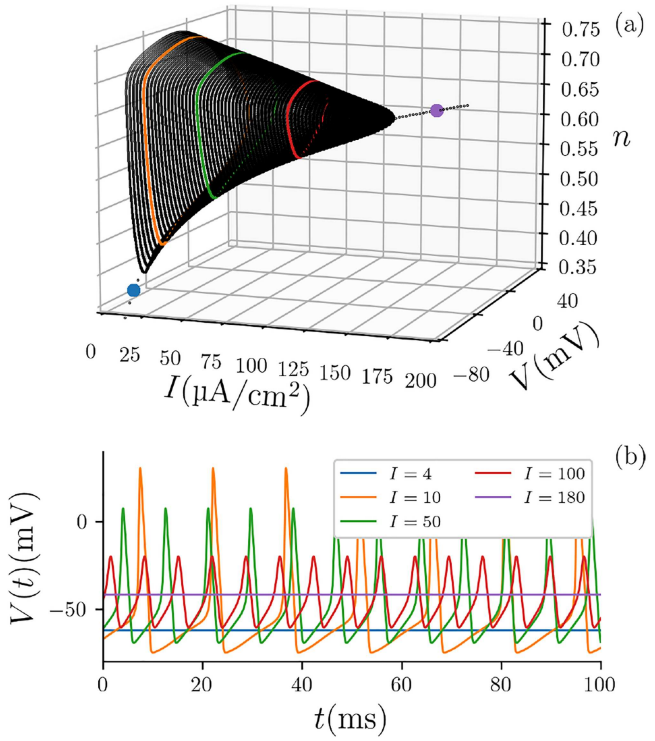

FIG. 1. Dynamics of the HH model under external constant current. (a) Two-dimensional projection $n \times V$ of the HH model for different values of I. We consider the set of constant values of Table I and the initial condition $V(0) = -70\text{mV}$ and $n(0) = m(0) = h(0) = 0$. A transient of 1s was discarded. (b) Time evolution of the membrane potential $V(t)$ for colored cases.

Figure 1 presents the evolution of a neuronal membrane in the model as a function of a constant external current $I_{\text{ext}}(t) = I$. The parameter I is a free parameter in the model and is measured in $\mu\text{A/cm}^2$. Table I shows the set of constant values considered in the simulation based on Ref. 13. Figure 1(a) depicts the two-dimensional projection $n \times V$ of the system phase portrait as a function of I. Figure 1(b) depicts the time evolution of $V(t)$ for colored cases shown in Fig. 1(a). The colors identify the membrane evolution submitted to $I = 4$ (blue), $I = 10$ (orange), $I = 50$ (green), $I = 100$ (red), and $I = 180$ (purple). As can be seen in the figures, constant values of membrane potential are observed for $I = 4$ (blue) and $I = 180$ (purple), while for the other values of external current, the membrane potential changes over time.

Considering I as a bifurcation parameter, the HH model is a classic dynamical system that undergoes Hopf bifurcations.[11] For small values of I, the system evolves to a stable equilibrium point (blue line). As I is increased, $I^* \approx 10$, the equilibrium point loses stability and gives rise to a stable limit cycle attractor due to a subcritical Andronov–Hopf bifurcation,[13] the limit cycle characterizes the periodic orbits of the spiking activity (orange, green, and red lines). The transition from the equilibrium state to the oscillatory state depends on the initial conditions for $I \approx I^*$.[21,22] As the magnitude of the injected current increases, the limit cycle is folded and the spiking dynamics collapse until the unstable equilibrium point becomes stable again (purple line) due to a supercritical Andronov–Hopf bifurcation point $(I^\dagger \approx 150)$.[13] The region that characterizes the limit cycle $I^* < I < I^\dagger$ delimits the excitation block of the neuron.[11] We observe an apparent amplitude × frequency relation in the excitation block; increasing I implies an increment of the frequency, but the price is paid in the decrease of the amplitude. The equations are integrated using the fourth-order Runge–Kutta method considering an integration step $\Delta t = 0.01\text{ms}$.

TABLE I. Constant values considered in the simulation of the Hodgkin–Huxley model.[13]

Membrane capacitance ($\mu\text{F/cm}^2$)	C_M	1
Maximum conductances (mS/cm^2)	g_{Na}	120
	g_K	36
	g_ℓ	0.3
Resting potentials (mV)	E_{Na}	50
	E_K	−77
	E_ℓ	−54.4

In this work, we focus on studying neuronal activity under external excitatory synaptic input due to the spontaneous activity coming from external subareas of the brain,[23] which means that we consider $I = 0$ (null constant current). These synapses are activated by random Poisson spike trains that reach the neuron with a constant mean rate ν_{ext}. The external synaptic current is the sum of the chemical excitatory signals given by

$$I_{\text{ext}}(t) = g_{\text{ext}}(E_{\text{syn}} - V)\sum_j s_j(t), \tag{11}$$

where g_{ext} is the external synaptic conductance, which is a free parameter measured in mS/cm^2, E_{syn} is the reversal potential ($E_{\text{syn}} = 40\text{mV}$), and s_j are the presynaptic signals from the neuron j. Every time t that a jth presynaptic spike occurs, $s(t)$ of the postsynaptic neuron is incremented from 0 by a difference of exponential functions,[13,24,25]

$$s(t) = \frac{\tau_0}{\tau_d - \tau_r}(e^{-t/\tau_d} - e^{-t/\tau_r}), \tag{12}$$

in which τ_0 is a unitary constant 1 ms, the decay time τ_d, and the rise time τ_r are constants of value 2.0 and 0.4 ms, respectively.

Figure 2 shows the dynamics of the HH model for different values of g_{ext} and a fixed external rate of the Poisson process $\nu_{\text{ext}} = 1$ spike/ms without the addition of a constant current. Figure 2(a) depicts the two-dimensional projection $n \times V$ of the HH model as a function of g_{ext}. Figure 2(b) presents the time evolution of $V(t)$ for the colored cases shown in Fig. 2(a). For conductance lower than $g_{\text{ext}} = 0.01$, the synaptic input is not sufficient to induce an action potential, and the membrane potential remains in a state close to the equilibrium point. Increasing the value of g_{ext}, the external Poissonian current produces irregular spikes, different from the case considering a constant current where periodic spikes are generated (Fig. 1). We also observe that for greater values of g_{ext}, the amplification of the synaptic current induces an increase in the spike

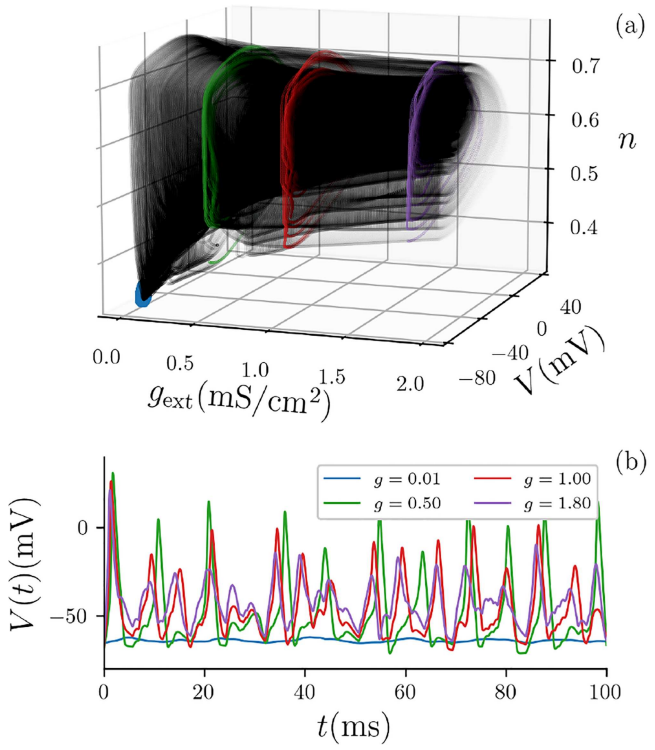

FIG. 2. Dynamics of the HH model under external synaptic current following a Poisson process and with a null constant baseline current $I = 0$. (a) Two-dimensional projection $n \times V$ of the system's phase portrait of the HH model for different values of g_{ext} for a fixed value of external rate $\nu_{ext} = 1$ spike/ms. (b) Time evolution of the membrane potential $V(t)$.

rate and a decrease in the amplitude of the neuronal oscillation, as well as considering an external constant current.

A more general framework for the spike frequency is presented in Fig. 3. Letting $\mathcal{F}$ the number of spikes in a second per simulation, Fig. 3 presents the mean value of $\mathcal{F}$, named $\langle\mathcal{F}\rangle$, which is the average over 100 different simulations as a function of the external conductance g_{ext} and the external rate ν_{ext}. The spike is detected when V crosses -20 mV with a positive derivative. It is expected that increasing both conductance g_{ext} and spiking external rate ν_{ext}, the dynamical behavior transits from a steady state (black region) to an oscillatory state (colored region). In addition, it is noted that there is compensation between ν_{ext} and g_{ext}. Furthermore, higher values of g_{ext} and ν_{ext} (a purple region located in the upper right) exhibit a decrease in $\langle\mathcal{F}\rangle$ corresponding to the saturation of the spiking activity illustrated in the purple line of Fig. 2 and can be related to the reduction of the limit cycle, which occurs for high values of external current I as shown in Fig. 1.

III. NETWORK SETUP AND SYNCHRONIZATION QUANTIFIER

To study the collective behavior of N coupled neurons, the membrane potential of each one is described by

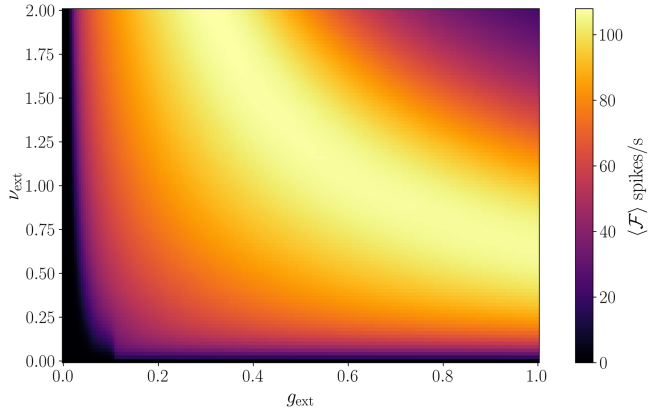

FIG. 3. The average spiking rate over 100 simulations under external excitatory synaptic input $\langle\mathcal{F}\rangle$.

$$C_M \frac{dV_i}{dt} = -g_K n_i^4 (V_i - E_K) - g_{Na} m_i^3 h_i (V_i - E_{Na}) - g_\ell (V_i - E_\ell) + I_{i,ext} + I_{i,coup}, \quad (13)$$

in which i is the neuronal index $i = 1, \ldots, N$; n_i, m_i, and h_i are given according to Eqs. (2)–(4), $I_{i,ext}$ is the external current arriving on each neuron i, and $I_{i,coup}$ is the synaptic coupled current, which presents a similar form as Eq. (11), given by

$$I_{i,coup}(t) = \varepsilon (E_{syn} - V_i) \sum_{j=1}^{N} a_{ij} r_j (V_j), \quad (14)$$

where ε is the coupling parameter; E_{syn} is the reversal synaptic potential; and $a_{i,j}$ is the element of the connection matrix, assuming $a_{i,j} = 1$ value if there is a connection from neuron j to neuron i, otherwise, $a_{i,j} = 0$. The variable r_i represents the fraction of bound receptors in the synapse where the kinetic model depends on the presynaptic neuron and is described by[26]

$$\frac{dr_i}{dt} = \left(\frac{1}{\tau_r} - \frac{1}{\tau_d}\right) \frac{1 - r_i}{1 + \exp[-(v_i(t) + 20)]} - \frac{r_i}{\tau_d}, \quad (15)$$

in which τ_r and τ_d are the same parameters as defined before.

We define the inter-spike-interval (ISI) of each neuron as the difference between its kth and $(k+1)$th spiking times,

$$ISI_{k,i} = t_{k+1,i} - t_{k,i}. \quad (16)$$

The coefficient of variation of the ISI can be defined as

$$CV = \sigma_{ISI}/\langle ISI \rangle, \quad (17)$$

where $\langle ISI \rangle$ is the mean value of all ISI and σ_{ISI} its standard deviation. The coefficient of variation of the ISI gives insights into the regularity of the neurons.[27]

To compute phase synchronization, we use the Kuramoto order parameter[28]

$$R = \left| \frac{1}{N} \sum_{j=1}^{N} e^{\imath \varphi_j(t)} \right|, \tag{18}$$

where φ_j is the phase of the jth neuron and $\imath = \sqrt{-1}$ here. In this case, $R = 1$ represents a completely phase-synchronized state in which all neurons spike at the same time. Conversely, $R = 0$ means that each neuron in the network has a corresponding pair that is completely out-of-phase, and this corresponds to a completely incoherent state (completely unsynchronized). In the case of a random distribution of N phases, the result would be $R \sim \sqrt{1/N}$.[29]

The use of the Kuramoto order parameter in studying neuronal dynamics involves associating a phase φ_i with the dynamics of individual neurons [Eq. (13)]. In this sense, there are several ways to do this association: the Hilbert transform,[30] the discrete and continuous wavelet transform,[31–33] and phase reduction models.[34,35] Here, we use the occurrence of each spike as an event to determine the phase of the neuron.[14] The spike occurs when the membrane potential cross a Poincaré section at $V = -20$ mV (with a positive derivative); with this, we have

$$\varphi_i(t) = 2\pi k_i + 2\pi \frac{t - t_{k,i}}{t_{k+1,i} - t_{k,i}}, \quad t_{k,i} \le t < t_{k+1,i}, \tag{19}$$

where $t_{k,i}$ represents the kth time in which the ith neuron spikes. The phase is increased by a factor of 2π for every spike.

IV. RESULTS

Throughout this paper, we consider a network with $N = 100$ randomly connected identical neurons, and the connections follow a uniform distribution. The connection probability is fixed in 10%, which means that on average, each neuron presents ≈ 10 random connections. We emphasize that the network activity is triggered by the external synaptic current [Eq. (11)] and coupling current [Eq. (14)], which means that null constant baseline current is applied in neurons. Considering the same external conductance g_{ext} and external rate ν_{ext} for all neurons, each neuron receives its own external Poissonian train of spikes $I_{i,\text{ext}}$. For simplicity, we have fixed the external rate of Poissonian spikes $\nu_{\text{ext}} = 1.0$ spike/ms giving us two free parameters: the coupling parameter ε and the external conductance g_{ext}. The phase synchronization is evaluated by averaging the Kuramoto order parameter over time, called the mean order parameter $\langle R \rangle$, for 10s after discarding 1 s to avoid transient effects, a time considered sufficient to obtain the asymptotic solution of the dynamic system and as a result of the other quantifiers used in this work. In addition, we compute the coefficient of variation of the inter-spike-intervals CV, defined in Eq. (17), and the mean firing rate $\langle \mathcal{F} \rangle$, which is the average over spikes produced by the network

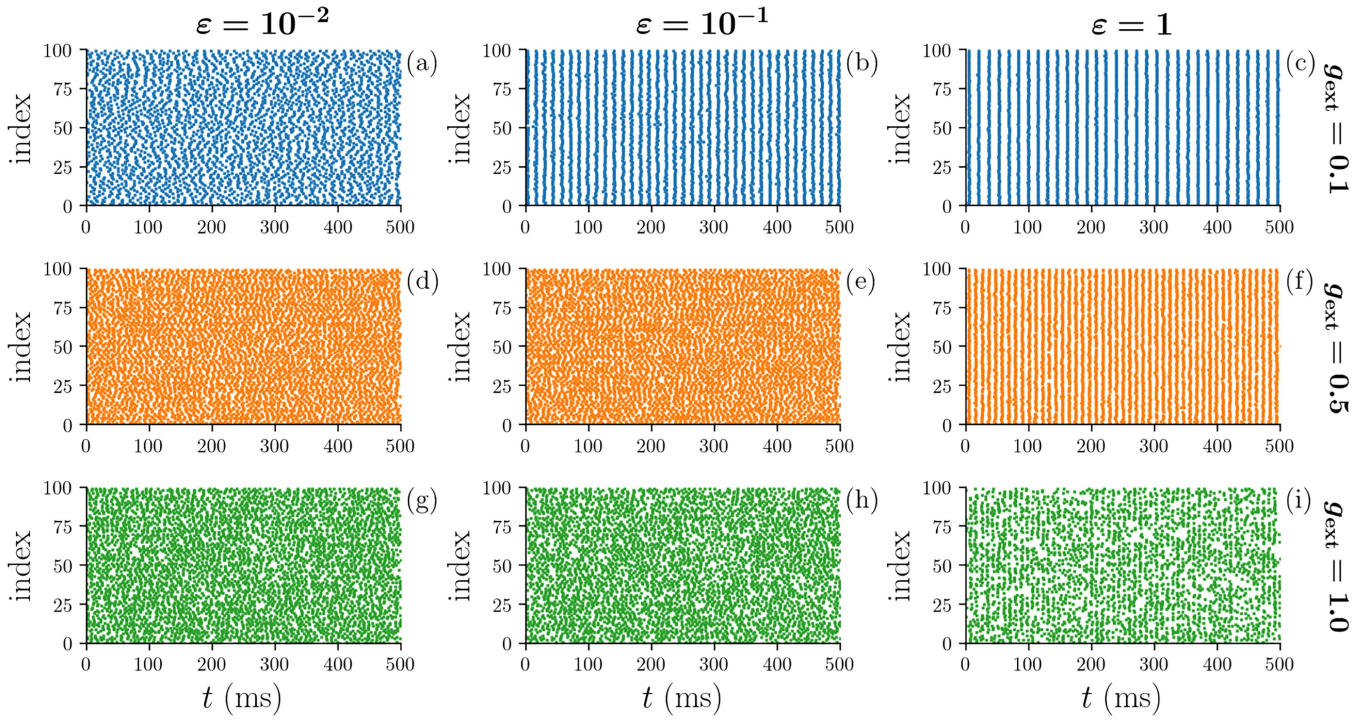

FIG. 4. Temporal evolution of the network. Raster plots of the network where each dot corresponds to the beginning of a spike. Panel (a) ($\varepsilon = 10^{-2}$, $g_{\text{ext}} = 0.1$), panel (b) ($\varepsilon = 10^{-1}$, $g_{\text{ext}} = 0.1$), panel (c) ($\varepsilon = 1$, $g_{\text{ext}} = 0.1$), panel (d) ($\varepsilon = 10^{-2}$, $g_{\text{ext}} = 0.5$), panel (e) ($\varepsilon = 10^{-1}$, $g_{\text{ext}} = 0.5$), panel (f) ($\varepsilon = 1$, $g_{\text{ext}} = 0.5$), panel (g) ($\varepsilon = 10^{-2}$, $g_{\text{ext}} = 1.0$), panel (h) ($\varepsilon = 10^{-1}$, $g_{\text{ext}} = 1.0$), and panel (i) ($\varepsilon = 1$, $g_{\text{ext}} = 1.0$).

per second. The initial conditions for the neurons of the network are randomly selected from $\{V_i \in [-80, 0]\,\text{mV}$ and $n_i, m_i, h_i \in [0, 1]\}$. To avoid any effect of the initialization in the results, all the surface values are an average of over ten different realizations considering distinct initial conditions and network configurations.

Figure 4 depicts raster plots of the network where each dot corresponds to the beginning of a spike for three different values of coupling $\varepsilon = 10^{-2}$ (left column), $\varepsilon = 10^{-1}$ (center column), and $\varepsilon = 1$ (right column) and for three values of external conductance $g_{\text{ext}} = 0.1$ (top row), $g_{\text{ext}} = 0.5$ (middle row), and $g_{\text{ext}} = 1.0$ (bottom row). Considering the top row, Figs. 4(a)–4(c) for $g_{\text{ext}} = 0.1$, when we increase the coupling from 10^{-2} to 10^{-1}, the network transits from the incoherent state to partial phase synchronization [indicated by the vertical structures in Fig. 4(b)] until the synchronized behavior for $\varepsilon = 1$ [magnified in Fig. 4(c)]. Furthermore, comparing Figs. 4(b) and 4(c), a decrease in spike occurrence is observed since the number of spike trains is smaller in Fig. 4(c). In the middle row, Figs. 4(d)–4(f) for $g_{\text{ext}} = 0.5$ due to the magnification of the external synaptic current, the transition for the synchronized state occurs only for higher values of coupling. In contrast, in the bottom row, Figs. 4(g)–4(i) for $g_{\text{ext}} = 1.0$, the increase of ε does not induce phase synchronization since the interplay of both external synaptic current and the coupling current saturates the spiking activity of the network.

The effect of the coupling ε in association with the external conductance g_{ext} is presented in a more general scheme in Fig. 5. Figure 5(a) exhibits the mean order parameter ($\langle R \rangle$), Fig. 5(b) shows the variability CV, and Fig. 5(c) shows the mean number of spikes in a second ($\langle \mathcal{F} \rangle$). The dark purple region in Fig. 5(a) exhibits low values of the order parameter $\langle R \rangle \approx 0$, which indicates incoherent behavior among neurons of the network. As the coupling increases, the network transitions to the phase synchronized regime (yellow region) $\langle R \rangle \approx 1$, at least for lower values of $g_{\text{ext}} < 0.7$. The onset of synchronization, which characterizes the transitions from an unsynchronized state to a synchronized state, is illustrated in red-orange colors ($\langle R \rangle \approx 0.5$). For higher values of g_{ext}, the stochasticity induced by the external current does not allow the network to phase synchronize. In Fig. 5(b), for $\varepsilon \approx 0$, the variability increases with the increment of g_{ext}. On the other hand, the variability decreases substantially, CV ≈ 0.05 for the most synchronized scenario $\langle R \rangle \approx 0.99$, which means that even for a high synchronized degree, the irregularity in the system does not allow completely periodic synchronization. In addition, Fig. 5(c), $\langle \mathcal{F} \rangle$ depicts non-monotonic evolution with the increase of ε (below the dashed line) and a monotonic decrease (above the dashed line). This peculiarity is discussed below.

As discussed in Sec. II, for fixed values of Table I, the activity of the neuron is determined by the current, which stimulates the neuron. In this sense, in the case of coupled neurons, the excitation of the neuron depends on the interplay of the coupling current (which comes from other neurons of the network) and the external synaptic currents (which are characterized by random spikes). $\bar{I}_{\text{ext}}$ and $\bar{I}_{\text{coup}}$ are the mean external and coupling currents over all neurons, respectively, defined by

$$\bar{I}_{\text{ext}}(t) = \frac{1}{N} \sum_i I_{i,\text{ext}}(t), \tag{20}$$

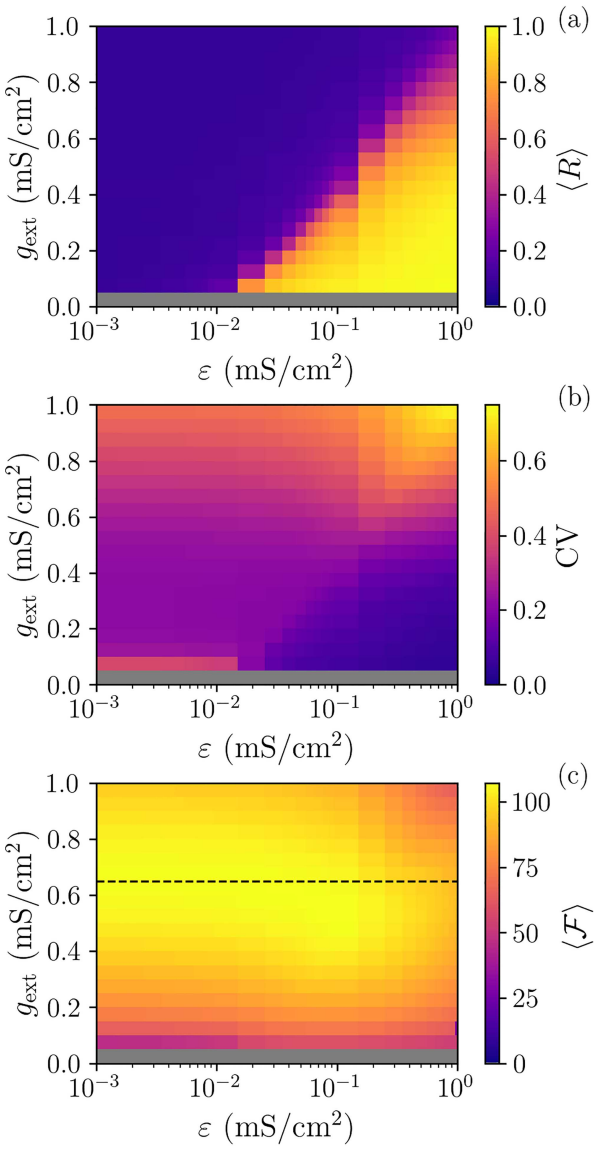

FIG. 5. (a) Mean order parameter $\langle R \rangle$, (b) the variability CV of inter-spike-intervals (ISIs), and (c) the mean network firing rate $\langle \mathcal{F} \rangle$ as a function of the coupling ε and the external conductance g_{ext}. The black dashed line delimits the non-monotonic behavior of $\mathcal{F}(\varepsilon)$ from the monotonic as ε increases. The gray area ($0 \leq g_{\text{ext}} \leq 0.05$) delimits the region where there is no spiking activity in the network.

$$\bar{I}_{\text{coup}}(t) = \frac{1}{N} \sum_i I_{i,\text{coup}}(t). \tag{21}$$

Moreover, it is possible to average these currents in time,

$$\langle \bar{I}_{\text{ext}} \rangle = \frac{1}{\tau} \sum_t \bar{I}_{\text{ext}}(t), \tag{22}$$

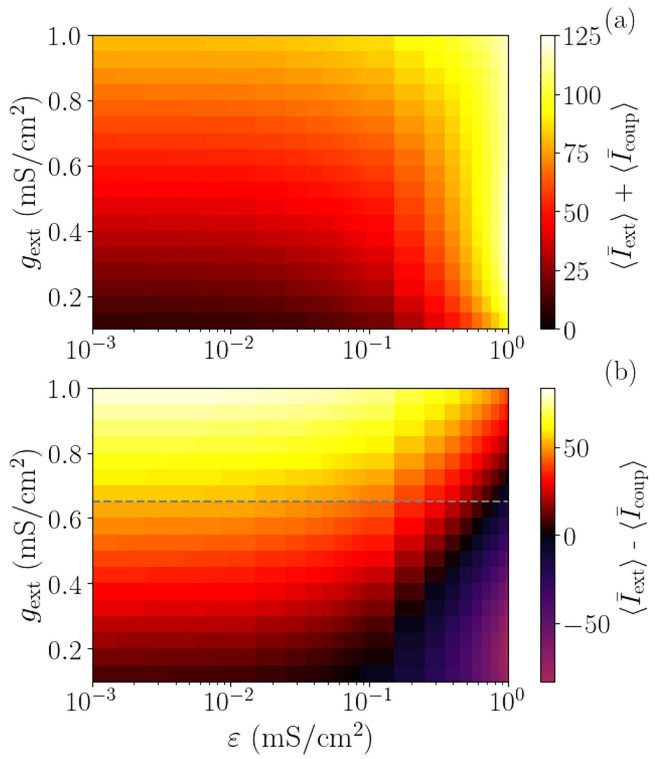

FIG. 6. Interplay between the external and internal coupling current parameters. (a) Sum over contributions $\langle \bar{I}_{ext} \rangle + \langle \bar{I}_{coup} \rangle$ and (b) subtraction $\langle \bar{I}_{ext} \rangle - \langle \bar{I}_{coup} \rangle$ as a function of the coupling ε and the external conductance g_{ext}. The dashed line in (b) delimits the region where the $\langle \bar{I}_{ext} \rangle \gtrsim \langle \bar{I}_{coup} \rangle$ for the whole interval of ε.

$$\langle \bar{I}_{coup} \rangle = \frac{1}{\tau} \sum_t \bar{I}_{coup}(t), \tag{23}$$

where τ corresponds to all-time instants after discarding 1 s to avoid transient effects. Hence, Eqs. (22) and (23) represent the mean contribution that each current performs to the network. Figure 6 presents in color codes in Fig. 6(a) the sum over contributions $\langle \bar{I}_{ext} \rangle + \langle \bar{I}_{coup} \rangle$ and Fig. 6(b) the subtraction $\langle \bar{I}_{ext} \rangle - \langle \bar{I}_{coup} \rangle$. Regarding Fig. 6(a), the total current increases with both the increment of g_{ext} and ε. On the other hand, in Fig. 6(b), it is noted that $\langle \bar{I}_{coup} \rangle$ gains relevance only in the purple region (lower right), which corresponds to the parameters in which the network presents relevant phase synchronization, as can be seen in Fig. 5(a). In addition, the dashed line in Fig. 6(b) delimits the region where the $\langle \bar{I}_{ext} \rangle \gtrsim \langle \bar{I}_{coup} \rangle$ for the whole interval of ε, which also delimits the boundary of the two distinct behaviors of $\langle \mathcal{F} \rangle$ with the increment of ε observed in Fig. 5(c). We also noted that greater values of coupling $\varepsilon > 1$ (not shown here) may lead to no spiking activity since the total current (external plus coupling) reaches high values, considerably reducing the number of spikes in the network.

The results so far indicate the effect of the balance between the external Poissonian signals and the internal coupling interaction of the network. Considering a null external current, $g_{ext} = 0$ (not shown here), there is no stimulation to start the spiking activity in the network, and it is no longer possible to associate a phase to the neurons. For slightly greater values, such as $g_{ext} > 0.05$, it is possible to start the activity in the network and the coupling can overcome the external current making a synchronized phase state possible. Conversely, at higher values of $g_{ext} > 0.6$, the stochasticity induced by the external Poissonian signals overcomes the coupling current preventing the network from synchronizing. The results can be explained by two aspects of the external synaptic current: First, the external current introduces *incoherence*, increasing the interspike interval (ISI) variability, as can be observed in Fig. 5(b). This is due to the influence of random Poissonian spikes, resulting in a higher degree of incoherence as the magnitude of the external current (g_{ext}) increases. Considering the theory of Kuramoto oscillators, the critical coupling that delimits the onset of synchronization depends on the frequency dispersion of the oscillators. The greater the dispersion of the frequencies, the higher the coupling parameter necessary to reach the phase synchronized state.[28] Therefore, the increase in incoherence makes the system hard to synchronize, which explains the increase in the critical coupling with the addition of g_{ext} observed in Fig. 5(a).

Second, a not-so-obvious effect of the external current is the *minimization of the coupling factor*, which occurs due to the supercritical Andronov–Hopf bifurcation of the Hodgkin–Huxley model. As observed in Fig. 2(b), higher values of g_{ext} decrease the amplitude of the spikes; hence, the signal emitted by the presynaptic neuron,

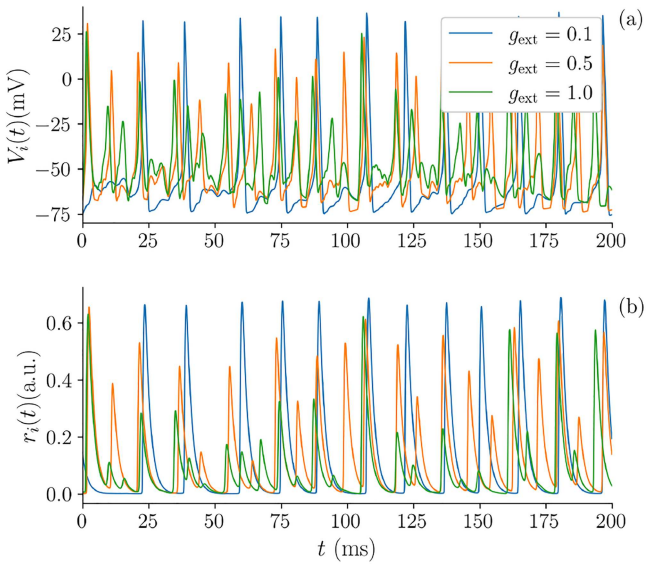

FIG. 7. Temporal evolution of the membrane potential (a) and the kinetic variable (b) of an isolated neuron for different values of g_{ext}. The increase in the magnitude of the external current minimizes the presynaptic effect, which is propagated to the network.

which is given by Eqs. (14) and (15), is minimized by the external current. To make the effect of minimization clearer, Fig. 7(a) presents the time evolution of the membrane potential of an isolated neuron, while Fig. 7(b) shows the kinetic variable r_i (signal emitted to postsynaptic neurons). We observe that for $g_{ext} = 0.1$ (blue), the amplitudes of both V_i and r_i are greater than the amplitude for higher values of $g_{ext} = 0.5$ (orange) and $g_{ext} = 1.0$ (green), which confirms the minimization effect of the external current on the coupling current.

In the context of this work, different investigation lines can be considered in the research. Stimulating only a subpopulation of a neural system has practical relevance in various scenarios. For instance, techniques, such as optogenetics, achieved through light-sensitive opsins introduced into targeted neurons, allow for the investigation of functional roles and interactions within the stimulated and non-stimulated subsets.[18,19] Similarly, in the studies of network of networks, targeted stimulation of specific regions or subsets provides insights into localized effects on synchronization and network-level properties, optimizing resource usage in large-scale networks.[20] With this in mind, one of the important questions is the following: What happens if only a fraction of the neurons of the network is available to receive external stimulation and the other fraction is influenced only by coupling with these neurons? We separate the network into two subgroups: the first group, named Group 1 (Ω_1), receives the external stimulation, while the second group, named Group 2 (Ω_2), $g_{ext} = 0$. This can be understood as if Group 1 shielded Group 2 from Poissonian spikes coming from the external environment.

Figure 8 presents the raster plots of the network considering half of the network in Group 1 (colored dots) and the other half in Group 2 (black dots). We consider three different values of coupling $\varepsilon = 3 \times 10^{-2}$ (left column), $\varepsilon = 5 \times 10^{-2}$ (center column), and $\varepsilon = 5 \times 10^{-1}$ (right column) and three values of external conductance $g_{ext} = 0.1$ (top row), $g_{ext} = 0.5$ (middle row), and $g_{ext} = 1.0$ (bottom row). It is observed in Fig. 8(a) incoherent behavior in neurons in Ω_1, while partial phase synchronization appears in neurons in Ω_2. This is an interesting phenomenon whereby the external current, which is necessary for the spiking activity in the network, overcomes the coupling current preventing phase synchronization in Ω_1. However, since neurons in Ω_2 are exposed only to the coupling factor, the spiking activity generated in Ω_1 is sufficient to generate spike activity and synchronize neurons in Ω_2. Hence, in this situation, it is possible to understand that the external Poissonian spikes induce incoherence spiking activity Ω_1 and spike activities in Ω_2 that are phase synchronized by the internal coupling. Increasing ε in Figs. 8(b) and 8(c), the coupling gains relevance, and both Ω_1 and Ω_2 transits to phase synchronization. In these cases, the internal coupling current is strong enough to synchronize

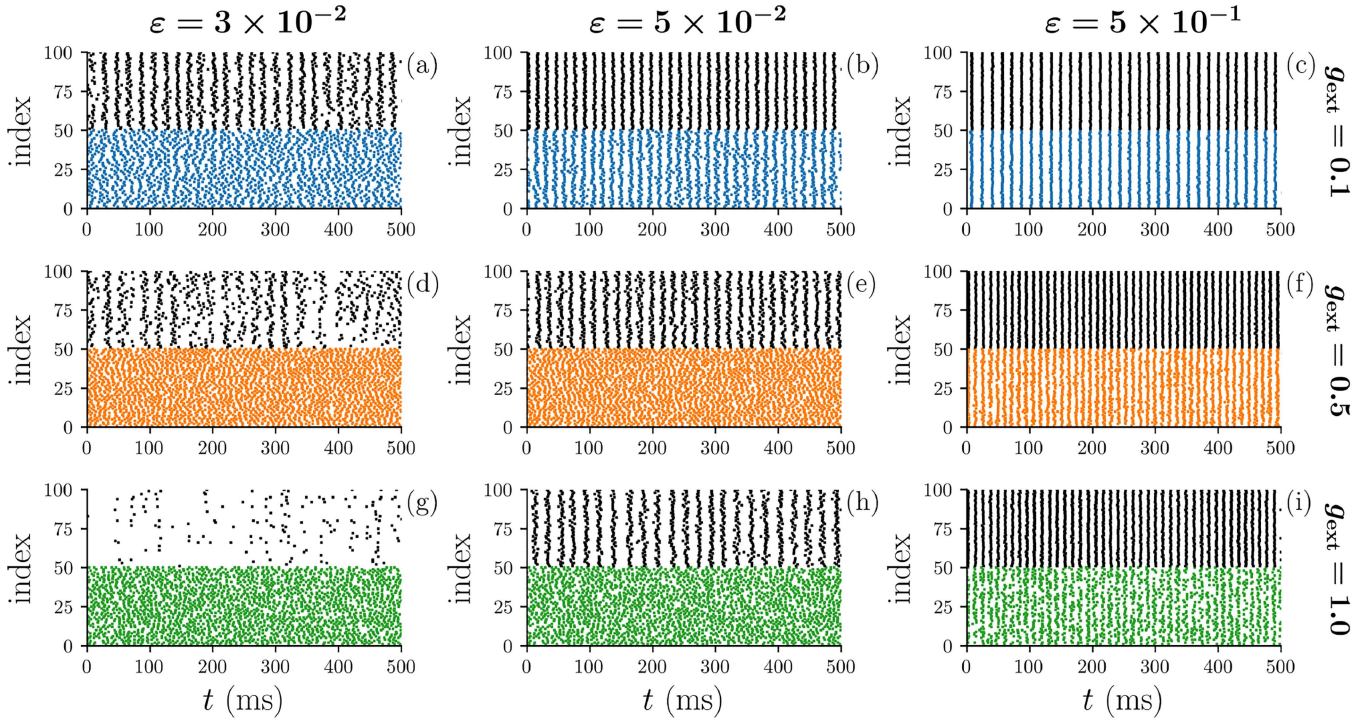

FIG. 8. Temporal evolution of the two subgroups, each one with and without Poissonian external signals. Raster plots of the network where each dot corresponds to a spike. We stimulate only half of the network. The stimulated neurons are represented in color codes, while the non-stimulated neurons are in black ones. Panel (a) ($\varepsilon = 3 \times 10^{-2}$, $g_{ext} = 0.1$), panel (b) ($\varepsilon = 5 \times 10^{-2}$, $g_{ext} = 0.1$), panel (c) ($\varepsilon = 5 \times 10^{-1}$, $g_{ext} = 0.1$), panel (d) ($\varepsilon = 3 \times 10^{-2}$, $g_{ext} = 0.5$), panel (e) ($\varepsilon = 5 \times 10^{-2}$, $g_{ext} = 0.5$), panel (f) ($\varepsilon = 5 \times 10^{-1}$, $g_{ext} = 0.5$), panel (g) ($\varepsilon = 3 \times 10^{-2}$, $g_{ext} = 1.0$), panel (h) ($\varepsilon = 5 \times 10^{-2}$, $g_{ext} = 1.0$), and panel (i) ($\varepsilon = 5 \times 10^{-1}$, $g_{ext} = 1.0$).

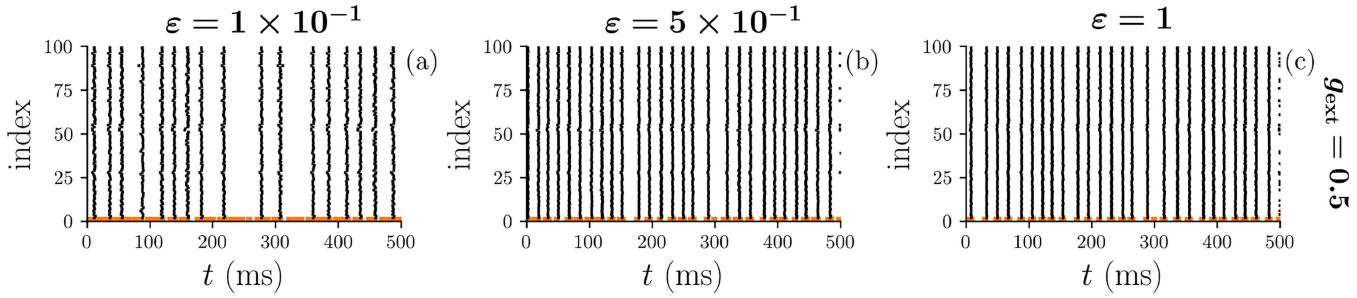

FIG. 9. Temporal evolution of the network by the Poissonian excitation in only one neuron. Raster plots of the network where each dot corresponds to a spike. The coupling parameter is the same for all neurons: (a) $\varepsilon = 1 \times 10^{-1}$, (b) $\varepsilon = 5 \times 10^{-1}$, and (c) $\varepsilon = 1$. We stimulate only one neuron, which is represented in orange color, while the non-stimulated neurons are represented in black ones. In this figure, g_{ext} is fixed in 0.5.

even Group 1 that is under competitive current input (external and internal).

As discussed before, there are two particular reasons why the increase in external current (g_{ext}) interferes with network coupling: incoherence and minimization. In this sense, Figs. 8(d)–8(f) and 8(g)–8(i) (middle and bottom rows) exhibit that increasing g_{ext} makes difficult the occurrence of synchronization, producing both groups with irregular spikes [Figs. 8(d) and 8(g)]. In addition, considering only the left column of Fig. 8, we observe that increasing g_{ext} decreases substantially the number of spikes of Ω_2, the fact that emphasizing the minimization of the internal coupling current that is dependent on the membrane potential values. On the other hand, increasing ε, one partially synchronized group (Ω_2) and one incoherent group (Ω_1) [Figs. 8(e) and 8(h)] are observed. In Fig. 8(f), both groups are partially synchronized, but Ω_1 is disturbed due to the external current. In Fig. 8(i), the higher external current values saturate the spiking activity in Ω_1 producing incoherence, while Ω_2 is synchronized. We also observe that lower values of coupling cannot be enough to activate the neurons in Ω_2.

A more extreme scenario is explored in Fig. 9, where we extrapolate the previous analysis by the excitation of only one neuron. For lower levels of coupling, $\varepsilon < 0.1$ (not shown), the neuron in Ω_1 spikes irregularly alone. For values greater than $\varepsilon = 0.1$, the coupling is high enough to produce spiking activity and sufficient to induce phase synchronization in Ω_2, as shown in Fig. 9(a). Increasing the coupling to $\varepsilon = 0.5$, as shown in Fig. 9(b), increases the number of spikes in Ω_2. The synchronization between Ω_1 and Ω_2 is greater in Fig. 9(b) when compared with Fig. 9(a) and even magnified in Fig. 9(c) $\varepsilon = 1$.

V. CONCLUSIONS

Throughout this paper, we have analyzed the phase-synchronization behavior of a network composed of 100 Hodgkin–Huxley neurons randomly coupled and submitted to external Poissonian signals. In this sense, when the coupling is turned off, we show a range of values in the external conductance that produces irregular spikes. Out of this range, due to the Hopf bifurcations of the Hodgkin–Huxley model (subcritical Andronov–Hopf bifurcation for lower values of I_{ext} and supercritical for greater values), there is no spiking activity: the reason is that for smaller values, the external current is not enough to stimulate the action potential of the neuron and greater values saturate the membrane potential preventing the neuron from spiking. We call the attention that distinct neuronal models may present different results, particularly if the studied model obtains distinct bifurcation points.[11]

In the presence of synaptic coupling, we take into account the interplay between the external Poissonian signals and the synaptic coupling currents. The process of phase synchronization (or partial phase synchronization) holds great physiological relevance, as it replicates the complex behavior of non-periodic neurons in real neural networks. In this scenario, phase synchronization occurs when the coupling current overcomes the external current, typically with small external conductance and significant coupling conductance. In this model, the increase in external conductance disrupts the synchronization in two different ways: through the irregularity of the random external spikes (incoherence) and the decrease in the amplitude of the presynaptic membrane potential (minimization) under high-intensity stimulation. In the same way, even considering the parameters in which the model presents a high degree of phase synchronization, the variability of the spikes indicates irregular behavior of the network. Additionally, the increase of the external current changes how the mean firing rate of the network evolves with the increment of the coupling, non-monotonic for lower values, and monotonic for greater values.

Last, we have analyzed the Poissonian excitation selectively applied to only a fraction of the neurons in the network, simulating a scenario where specific neural subpopulations receive external signals, while others remain shielded from this stimulation. This approach replicates real-world situations where certain neural regions or cell groups are subject to external influences, while others are not. In this case, we have shown that when only half of the network is stimulated, it is possible to induce phase synchronization in the non-stimulated group, while the stimulated one is in incoherent behavior. The phase synchronization of the whole network can be reached by increasing the coupling parameter. A different scenario is reached for greater values of the external conductance, where the coupling current is minimized by the reduction of potential membrane oscillations due to the external current, making it possible to disrupt the synchronization even in the non-stimulated part of the network. We also studied the case where only one neuron is stimulated. In this case, for sufficient values of coupling, it is possible

to generate spiking activity in the network, which due to the coupling current is accompanied by synchronization behavior. Future works will be devoted to exploring how the spiking activity and phase synchronization rises considering the analytical approaches suggested in Refs. 28, 32, 34, and 36–40.

ACKNOWLEDGMENTS

B.R.R.B., E.E.N.M., and P.R.P. acknowledge the support of the São Paulo Research Foundation (FAPESP), Brazil (Proc. 2018/03211-6, 2020/04624-2, 2021/09839-0, and 2022/05153-9) and Financiadora de Estudos e Projetos (FINEP). M.H. was funded by national funds through the FCT—Fundação para a Ciência e a Tecnologia, I.P., under the scope of the projects UIDB/00297/2020 and UIDP/00297/2020 (Center for Mathematics and Applications). J.O. and A.C.A. are financed by the Coordenação de Aperfeiçoamento de Pessoal de Nível Superior—Brasil (CAPES)—Finance Code 001 (Proc. 88887.603065/2021-00 and 88887.715012/2022-00).

AUTHOR DECLARATIONS

Conflict of Interest

The authors have no conflicts to disclose.

Author Contributions

Bruno R. R. Boaretto: Conceptualization (equal); Data curation (equal); Investigation (equal); Methodology (equal); Validation (equal); Visualization (equal); Writing – original draft (equal); Writing – review & editing (equal). **Paulo R. Protachevicz:** Conceptualization (equal); Investigation (equal); Validation (equal); Visualization (equal); Writing – original draft (equal); Writing – review & editing (equal). **Matheus Hansen:** Conceptualization (equal); Investigation (equal); Methodology (equal); Validation (equal); Visualization (equal); Writing – original draft (equal); Writing – review & editing (equal). **Jonas Oliveira:** Conceptualization (equal); Validation (equal); Visualization (equal); Writing – review & editing (equal). **Alexandre C. Andreani:** Conceptualization (equal); Visualization (equal); Writing – original draft (equal); Writing – review & editing (equal). **Elbert E. N. Macau:** Conceptualization (equal); Data curation (equal); Methodology (equal); Project administration (equal); Supervision (equal); Validation (equal); Visualization (equal); Writing – original draft (equal); Writing – review & editing (equal).

DATA AVAILABILITY

The data that support the findings of this study are available from the corresponding author upon reasonable request.

REFERENCES

[1] E. R. Kandel, J. H. Schwartz, T. M. Jessell, S. A. Siegelbaum, and A. J. Hudspeth, *Principles of Neural Science*, 5th ed. (McGraw-Hill, New York, 2013).
[2] W. R. Softky and C. Koch, "The highly irregular firing of cortical cells is inconsistent with temporal integration of random EPSPs," J. Neurosci. **13**, 334–350 (1993).
[3] E. Schneidman, W. Bialek, and M. J. Berry, "Synergy, redundancy, and independence in population codes," J. Neurosci. **23**, 11539–11553 (2003).
[4] N. Brunel and V. Hakim, "Fast global oscillations in networks of integrate-and-fire neurons with low firing rates," Neural Comput. **11**, 1621–1671 (1999).
[5] M. N. Shadlen and W. T. Newsome, "The variable discharge of cortical neurons: Implications for connectivity, computation, and information coding," J. Neurosci. **18**, 3870–3896 (1998).
[6] C. F. Stevens and A. M. Zador, "Input synchrony and the irregular firing of cortical neurons," Nat. Neurosci. **1**, 210–217 (1998).
[7] A. Mazzoni, S. Panzeri, N. K. Logothetis, and N. Brunel, "Encoding of naturalistic stimuli by local field potential spectra in networks of excitatory and inhibitory neurons," PLoS Comput. Biol. **4**, e1000239 (2008).
[8] A. Renart, J. De La Rocha, P. Bartho, L. Hollender, N. Parga, A. Reyes, and K. D. Harris, "The asynchronous state in cortical circuits," Science **327**, 587–590 (2010).
[9] A. Litwin-Kumar and B. Doiron, "Slow dynamics and high variability in balanced cortical networks with clustered connections," Nat. Neurosci. **15**, 1498–1505 (2012).
[10] A. L. Hodgkin and A. F. Huxley, "A quantitative description of membrane current and its application to conduction and excitation in nerve," J. Physiol. **117**, 500 (1952).
[11] E. M. Izhikevich, *Dynamical Systems in Neuroscience* (MIT Press, 2007).
[12] J. Keener and J. Sneyd, *Mathematical Physiology* (Springer-Verlag, New York, 1998).
[13] B. Ermentrout and D. H. Terman, *Mathematical Foundations of Neuroscience* (Springer, 2010), Vol. 35.
[14] M. V. Ivanchenko, G. V. Osipov, V. D. Shalfeev, and J. Kurths, "Phase synchronization in ensembles of bursting oscillators," Phys. Rev. Lett. **93**, 134101 (2004).
[15] F. Mormann, K. Lehnertz, P. David, and C. E. Elger, "Mean phase coherence as a measure for phase synchronization and its application to the EEG of epilepsy patients," Phys. D: Nonlinear Phenom. **144**, 358–369 (2000).
[16] C. Hammond, H. Bergman, and P. Brown, "Pathological synchronization in Parkinson's disease: Networks, models and treatments," Trends Neurosci. **30**, 357–364 (2007).
[17] O. V. Popovych and P. A. Tass, "Control of abnormal synchronization in neurological disorders," Front. Neurol. **5**, 268 (2014).
[18] K. Deisseroth, "Optogenetics," Nat. Methods **8**, 26–29 (2011).
[19] O. Yizhar, L. E. Fenno, T. J. Davidson, M. Mogri, and K. Deisseroth, "Optogenetics in neural systems," Neuron **71**, 9–34 (2011).
[20] E. L. Lameu, F. S. Borges, R. R. Borges, K. C. Iarosz, I. L. Caldas, A. M. Batista, R. L. Viana, and J. Kurths, "Suppression of phase synchronisation in network based on cat's brain," Chaos **26**, 043107 (2016).
[21] A. V. Andreev, N. S. Frolov, A. N. Pisarchik, and A. E. Hramov, "Chimera state in complex networks of bistable Hodgkin-Huxley neurons," Phys. Rev. E **100**, 022224 (2019).
[22] M. Hansen, P. R. Protachevicz, K. C. Iarosz, I. L. Caldas, A. M. Batista, and E. E. N. Macau, "Dynamics of uncoupled and coupled neurons under an external pulsed current," Chaos, Solitons Fractals **155**, 111734 (2022).
[23] G. B. Ermentrout, R. F. Galán, and N. N. Urban, "Reliability, synchrony and noise," Trends Neurosci. **31**, 428–434 (2008).
[24] N. Brunel and X. Wang, "What determines the frequency of fast network oscillations with irregular neural discharges? I. Synaptic dynamics and excitation-inhibition balance," J. Neurophysiol. **90**, 415–430 (2003).
[25] S. Cavallari, S. Panzeri, and A. Mazzoni, "Comparison of the dynamics of neural interactions between current-based and conductance-based integrate-and-fire recurrent networks," Front. Neural Circuits **8**, 12 (2014).
[26] A. Destexhe, Z. F. Mainen, and T. J. Sejnowski, "An efficient method for computing synaptic conductances based on a kinetic model of receptor binding," Neural Comput. **6**, 14–18 (1994).
[27] C. Pélabon, C. H. Hilde, S. Einum, and M. Gamelon, "On the use of the coefficient of variation to quantify and compare trait variation," Evol. Lett. **4**, 180–188 (2020).
[28] Y. Kuramoto, "Self-entrainment of a population of coupled non-linear oscillators," in *International Symposium on Mathematical Problems in Theoretical Physics* (Springer, 1975), pp. 420–422.
[29] A. Arenas, A. Díaz-Guilera, J. Kurths, Y. Moreno, and C. Zhou, "Synchronization in complex networks," Phys. Rep. **469**, 93–153 (2008).

[30]A. Pikovsky, M. Zaks, M. Rosenblum, G. Osipov, and J. Kurths, "Phase synchronization of chaotic oscillations in terms of periodic orbits," Chaos **7**, 680–687 (1997).
[31]A. Koronovskii and A. Hramov, "Chaotic phase synchronization studied by means of continuous wavelet transform," Tech. Phys. Lett. **30**, 587–590 (2004).
[32]S. Hata, T. Shimokawa, K. Arai, and H. Nakao, "Synchronization of uncoupled oscillators by common gamma impulses: From phase locking to noise-induced synchronization," Phys. Rev. E **82**, 036206 (2010).
[33]M. T. Ferreira, R. Follmann, M. O. Domingues, E. E. Macau, and I. Z. Kiss, "Experimental phase synchronization detection in non-phase coherent chaotic systems by using the discrete complex wavelet approach," Chaos **27**, 083122 (2017).
[34]P. Danzl, R. Hansen, G. Bonnet, and J. Moehlis, "Partial phase synchronization of neural populations due to random Poisson inputs," J. Comput. Neurosci. **25**, 141–157 (2008).
[35]A. Pérez-Cervera, B. Lindner, and P. J. Thomas, "Quantitative comparison of the mean–return-time phase and the stochastic asymptotic phase for noisy oscillators," Biol. Cybern. **116**, 219–234 (2022).
[36]D. Roy, A. Ghosh, and V. K. Jirsa, "Phase description of spiking neuron networks with global electric and synaptic coupling," Phys. Rev. E **83**, 051909 (2011).
[37]N. Brunel, "Dynamics of sparsely connected networks of excitatory and inhibitory spiking neurons," J. Comput. Neurosci. **8**, 183–208 (2000).
[38]S. Petkoski, D. Iatsenko, L. Basnarkov, and A. Stefanovska, "Mean-field and mean-ensemble frequencies of a system of coupled oscillators," Phys. Rev. E **87**, 032908 (2013).
[39]J. A. Acebrón, L. L. Bonilla, C. J. P. Vicente, F. Ritort, and R. Spigler, "The Kuramoto model: A simple paradigm for synchronization phenomena," Rev. Mod. Phys. **77**, 137 (2005).
[40]L. Muller, J. Mináč, and T. T. Nguyen, "Algebraic approach to the Kuramoto model," Phys. Rev. E **104**, L022201 (2021).